Conference on Modelling Fluid Flow (CMFF'25)
The 19th International Conference on Fluid Flow Technologies
Budapest, Hungary, August 26 - August 29, 2025

ESTIMATION OF RELATION BETWEEN PRESSURE DIFFERENCE AND FLOW RATE IN A FRANCIS-TURBINE SPIRAL CASE USING NUMERICAL COMPUTATION

Muris TORLAK[1], Adis BUBALO[2], Ehlimana JUGO[3], Safet ISIĆ[4]

[1] Corresponding Author. Department of Energy, Process Technology and Environmental Engineering, Faculty of Mechanical Engineering, University of Sarajevo. Vilsonovo šetalište 9, BA-71000 Sarajevo, Bosnia and Herzegovina. Tel.: +387 62 14 00 77, E-mail: torlak@mef.unsa.ba
[2] JP Elektroprivreda BiH dd Sarajevo, Podružnica Hidroelektrane na Neretvi. Jaroslava Černija 1, BA-88420 Jablanica, Bosnia and Herzegovina. E-mail: a.bubalo@epbih.ba
[3] Department of Energy, Process Technology and Environmental Engineering, Faculty of Mechanical Engineering, University of Sarajevo. Vilsonovo šetalište 9, BA-71000 Sarajevo, Bosnia and Herzegovina. E-mail: jugo@mef.unsa.ba
[4] Corresponding Author. Faculty of Mechanical Engineering, University "Džemal Bijedić" of Mostar. University Campus, BA-88104 Mostar, Bosnia and Herzegovina. Tel.: +387 62 99 48 77, E-mail: safet.isic@unmo.ba

ABSTRACT

Pressure differences at given locations along radial direction on the walls of the spiral casing of a hydraulic turbine, anticipated for the use in Winter-Kennedy measuring, are computed for a range of water flow rates through the turbine. Different types of boundary condition at the stay-vane side (zero-gradient outlet, average pressure, integral flow rate) are tested first. Several approaches to turbulence handling are also investigated (eddy-viscosity models: realizable k-ε and k-ω SST, then elliptic-blending Reynolds-stress model, as well as large-eddy simulation without subgrid-scale modelling). The simulations are done for a case from an operating hydropower plant, and the results are compared to the pressure values measured in the spiral casing and the flow rates obtained from the recorded output power of the electric generator in real working conditions. The results of numerical simulation agree very well with the measured pressure values. Consequently, a relation between the pressure difference at the monitoring points and the incoming flow rate is established in the form of a power function.

Keywords: computational fluid dynamics (CFD), flow rate measuring, hydraulic turbines, hydropower plants, Winter-Kennedy method

NOMENCLATURE

D	$[m]$	inner diameter of the inlet pipe
P_T	$[W]$	turbine output power
Q	$[m^3/s]$	flow rate
c	[-]	a coefficient of proportionality
g	$[m/s^2]$	gravitational acceleration
h	$[m]$	net head
n	[-]	exponent
p	$[Pa]$	static pressure
t	$[s]$	time
y^+	[-]	non-dimensional wall distance
z_{ps}	$[m]$	vertical position of the pressure sensor
Δ		operator of subtraction, difference
η_T	[-]	turbine efficiency
ρ	$[kg/m^3]$	water density

1. INTRODUCTION

Output power of water turbines is a time-dependent function of the available water net head in a power plant, the water flow rate, and the turbine efficiency, which is usually written in form such as in Eq. (1):

$$P_T(t) = \rho\, g\, h\big(Q(t)\big)\, Q(t)\, \eta_T\big(Q(t)\big)\,. \qquad (1)$$

Time variation of the turbine output power is imposed by electric-grid demands. Neither net head nor turbine efficiency can be directly controlled and varied during regular everyday turbine operation. Practically, the only remaining quantity to control and adapt the turbine output power is the flow rate. The output power is directly dependent on the flow rate Q, but variation of the flow rate also produces variable power losses, affecting thus the net head and the turbine efficiency. Hence, monitoring and management of the water turbines' performance

require reliable estimation of the water flow rate during their operation.

One of the methods used for measuring water flow rate in hydropower plants is the Winter-Kennedy method [1-8]. The method is based on action of centrifugal forces in curved pipes or ducts. The centrifugal forces result in increase of static pressure on the outer side of the curved pipe, and its decrease on the inner side of the pipe. In theory, the pressure difference in radial direction is proportional to the square of the mean velocity of flow through the pipe, thus it is proportional to the square of the flow rate. Accordingly, the dependence of the flow rate on the radial pressure difference is described by Eq. (2):

$$Q = c\,(\Delta p)^n\,. \qquad (2)$$

Theoretically, the exponent n is equal to 0.5, while the coefficient c is a positive real number describing the fluid properties, the geometric properties, and real conditions of the curved pipe. In reality, complex shapes and other geometric properties, such as surface irregularities, roughness, flow regime etc., yield certain deviations from theoretical values, so in practice $n \neq 0.5$.

By measuring Δp, one can get the information on the flow rate using the relation Eq. (2). The method is simple, it does not require moving parts, it is not invasive in the pipe flow, so it does not trigger additional energy loss. It can be applied continuously during the operation. In hydropower plants pressure measuring is installed on spiral casing of a turbine. However, the method requires reliable *a priori* calibration of the coefficients c and n for each specific turbine, usually by (model) experiments in the lab conditions.

Accuracy of water pressure measurement in realistic operational conditions in the spiral casings of hydraulic turbines may decrease over long time periods. This may be a consequence of water debris, sedimentation in the pipe interior, malfunction of an element in the measuring system, occurrence of local pressure variations due to temporary irregular flow patterns etc. Therefore, use of numerical simulation to establish pressure – flow-rate relation for the purpose of flow-rate assessment in operating conditions, or some of protective functions, can be important and improve working processes in hydroelectric power plants.

In this paper a method to obtain coefficients in relation of the pressure difference and the water flow rate in a spiral case of a water turbine by computer simulation using computational fluid dynamics (CFD) instead of experimental calibration is investigated.

2. METHOD

Relation between flow rate and radial pressure difference, as anticipated for use with Winter-Kennedy method, is investigated in case of a real Francis turbine of a medium-head hydropower plant.

Computer program Simcenter STAR-CCM+ [9] is used for meshing, computing, and visualization, where a finite-volume method is applied to discretize the balance equations of mass and momentum, as well as turbulence transport equations (where these are used). Thus obtained systems of linear equations are solved by an algebraic-multigrid method.

Water is considered as incompressible, viscous fluid. The flow field is calculated in parallel using 6 processors for steady-state runs or 64 processors for time-dependent runs. For a series of prescribed water flow rates, the pressure values are evaluated at the monitoring points, corresponding to the locations used in Winter-Kennedy measuring method [1-2], see Figure 1.

Verification of the results is done comparing the results with the data recorded in the power plant in real conditions or the data calculated from them.

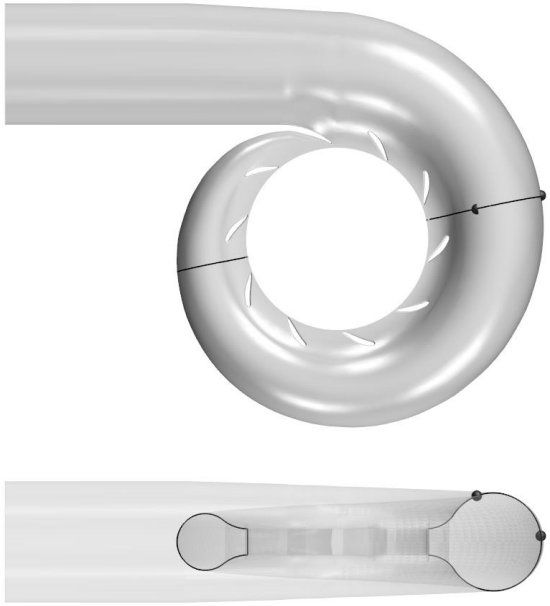

Figure 1. Geometric model of the spiral casing, with the pressure monitoring locations indicated (dark-grey points): the top view (above) and the horizontal view perpendicular to the axis of the inlet pipe, with the section through the monitoring points (below)

2.1. Computational setup

In order to increase the overall processing speed the computational domain is focused on spiral casing, including stay vanes, Fig. 1. The guide vanes and the turbine runner are avoided. Instead, outflow boundary of cylindrical shape is created in the region between the stay vanes and the guide vanes.

The geometric model of the spiral casing is obtained by 3D scanning from the interior (this can be done, for example, during a regular inspection period, when the spiral casing and the turbine are

empty). The resulting point cloud is used to create an appropriate triangulated surface.

The inflow boundary (not shown in figure) is defined as a perpendicular cross section of the inlet pipe, located 4*D* upstream from the entrance to the spiral casing. At the inflow boundary, integral flow rate is prescribed and kept constant in every single calculation run. Spiral casing and stay vanes are considered as fixed, impermeable no-slip walls. Hence, both the tangential and normal component of velocity are set to zero. The wall pressure values are obtained by extrapolation from the near-wall cells.

Three different types of boundary condition are tested at the outflow boundary, in the region between the stay vanes and guide vanes: (a) integral flow rate with specified slope of flow direction, (b) developed outlet flow (with local flow directions extrapolated from the domain interior and zero-gradient condition of physical quantities), and (c) specified *surface-averaged* pressure over the boundary.

The computational mesh inside the CAD model is automatically generated and refined depending on the boundaries' curvature, see Figure 2. The mesh consists of cubic cells, trimmed near the boundaries to adapt to their shape, and 20 layers of prisms along the walls in order to capture velocity gradients in the boundary layer regions. The final mesh contains about 5 030 000 cells.

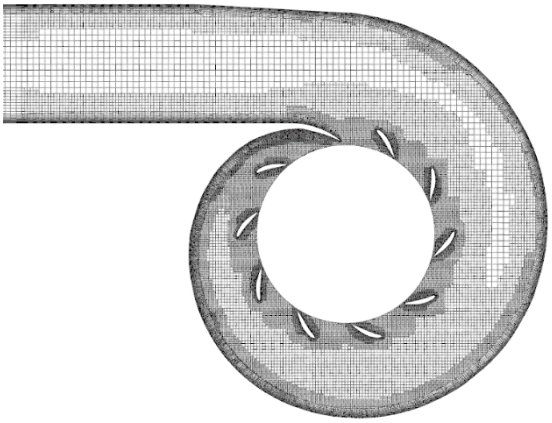

Figure 2. Computational mesh in the horizontal section plane of the spiral casing

Turbulence is resolved using: realizable k-ε model [10] (in this paper also denoted as R KE), k-ω SST model [11] (denoted as KW SST), elliptic-blending Reynolds-stress model [12] (EB RSM), and large-eddy simulation without subgrid-scale modelling (denoted as LES or LES w/o SGS). Implementations of all Reynolds-averaged Navier-Stokes equations (RANS) models used in this work are capable of handling a wide range of y^+ values, from viscous sublayer to logarithmic region. LES w/o SGS reduces, practically, to solution of laminar-flow model, so its wall boundary condition does not involve any special wall treatment and wall distance was not calculated.

Although, formally, LES methods require much finer spatial resolution than RANS models, for sake of keeping computing costs and time demands reduced, LES w/o SGS is done on the same mesh as the RANS models, yielding thus comparison of results obtained with conditions the same or similar, as much as possible.

All simulations are done aiming at steady-state scenario, so the RANS models (R KE, KW SST, and EB RSM) are run ignoring the time dimension and the inertial contribution to the balance of forces, while LES, as imposed by the model, is run in time. Once again, all boundary conditions are kept constant. Since the final solution is expected to be stationary, in case of LES the inertial term of the momentum equation is first discretized by 1st-order accurate implicit Euler scheme, and the time step of 0.005 *s* was adopted, to provide some numerical damping while marching in time. Also convective term is discretized by 1st-order accurate upwind scheme at the beginning. In order to refine the computation, discretization order is increased during simulation (described later in the text), typically after 2 *s* to 3 *s* of simulated time, depending on the flow rate. For the details on numerical methods and discretization techniques the reader is referred to, for example, the books [13, 14] or the software documentation [9].

2.2. Reference measuring

The pressure in the spiral case is measured on a turbine operating in real conditions, at two points along the same radial section, already shown in Fig. 1. Pressure transducers with strain gauges, a measuring range of 0–20 *bar*, accuracy class 0.3, and nominal sensitivity of 0.2 *mV*/*bar*, are used. One transducer is calibrated using a hydraulic scale with an accuracy class of 0.1, and the sensitivity of the second sensor is adjusted to match the readings of the first one. The measurement signal is acquired and amplified by a SPIDER8 amplifier and recorded using CATMAN software [15]. The pressure difference is measured during stationary turbine operation at seven different power levels, ranging from 12 *MW* to 30 *MW*. Power stabilization and achievement of conditions for pressure measurement is monitored by measuring the signal from the opening grade of the turbine guide vanes.

Due to different vertical positions of the two paired sensors, gravity-induced pressure difference is obtained in the recorded values. These are corrected through manual calculation, subtracting the gravity contribution $\rho g \Delta z_{ps}$.

In addition to the pressure differences, a number of corresponding operating data is recorded, including net head, and the output power of the electric generator.

For the reference and comparison with the simulated results, the flow rate is not directly measured, but it is found through a "backward"-calculation from the recorded generator output-power, which is a common procedure for hydraulic turbines in operating conditions. One takes into account efficiency of the generator, power losses in mechanical transmission, and the efficiency of the turbine (from the corresponding hill chart, for the given net head and vane opening). Thus, the input power of the turbine P_T/η_T is obtained, from which the water flow rate is obtained using Eq. (1) having the net head known.

3. RESULTS

In Figure 3 the results of computer simulation are shown for two different types of the outflow boundary condition: zero-gradient outlet and constant average pressure, both of them computed with R KE turbulence model. The reference values – the measured pressure difference and the corresponding flow-rate calculated from the recordings in the power-plant – are shown as well. Both boundary conditions provide the expected trend of the pressure-difference variation. Deviations of the results obtained with zero-gradient outlet condition from the reference data exhibit overestimation in the entire range of the observed flow rates, and are larger than deviations arising in use of average-pressure condition. For both types of boundary condition, the deviations increase with the increase of the flow rate. The computations with the integral flow-rate condition with specified flow direction at the outflow boundary are not shown in the diagram, but they yield the results similar to those achieved with average-pressure condition.

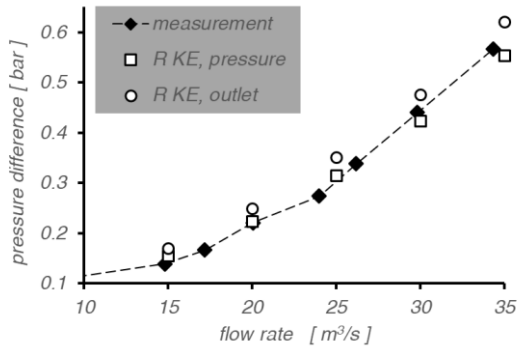

Figure 3. Comparison of average-pressure and zero-gradient-outlet boundary condition

Figure 4 shows a comparison of the results obtained with different types of turbulence modelling applied to the case with the average-pressure outflow boundary condition. The results are quite close to each other, and they are very close to the reference data. This allows conclusion that the choice of turbulence model is not decisive for the overall flow behaviour reflected in the observed pressure-difference and flow-rate relation.

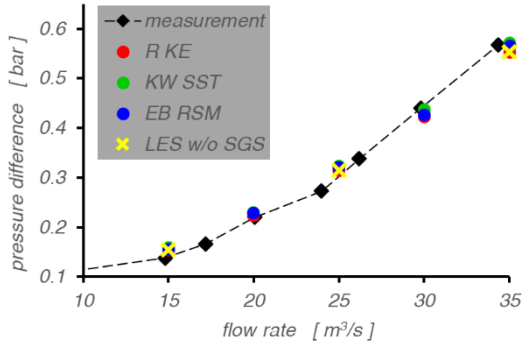

Figure 4. Different turbulent flow simulations with average-pressure outflow boundary

The trend of the curves in Figs. 3 to 4, representing the computational results, approximates quadratic parabola, as expected. By fitting a curve in form of Eq. (2) through the these data (i.e. through arithmetic average of results obtained with different turbulence models for each single flow rate), including corrective translation along the Δp-axis, which accounts for the part of pressure difference caused by gravitational effect and difference in pressure-sensor elevations $\rho g \Delta z_{ps}$, one can obtain the relation:

$$Q = 49.6392 \left(\frac{\Delta p - \rho g \Delta z_{ps}}{100\,000} \right)^{0.5004} . \qquad (3)$$

Note that this relation holds only for the speific spiral casing geometry in the presented simulations. Eq. (3) delivers an error less than 0.5% as compared to the flow rates at sampling points (simulated results).

Fitting a curve of the same form through the measured data delivers the relation:

$$Q = 46.1312 \left(\frac{\Delta p - \rho g \Delta z_{ps}}{100\,000} \right)^{0.4348} . \qquad (4)$$

The resulting exponent in Eq. (4) is clearly lower than the theoretical one. This can be addressed to realistic conditions in the measurement, such as wall roughness and other sources of energy losses. On the other hand, simulation does not take these into account, so the relation resulting from fitting of simulation data has the exponent much closer to the ideal conditions.

Figure 5 shows convergence history of simulations with R KE turbulence model for the minimum (above) and the maximum (below) flow rate from the investigated range, Q=15 m^3/s and Q=35 m^3/s respectively, using all three types of outflow boundary condition. While the average-pressure and the integral flow-rate boundary condition show very similar convergence behaviour,

the zero-gradient outlet condition shows again an overestimation. According to the case of the lowest flow rate (Fig. 5, above), the rate at which the final result is approached is the fastest (i.e. it is achieved in the fewest number of iterations) in the condition of flow-rate with the prescribed flow direction (about 500 iterations).

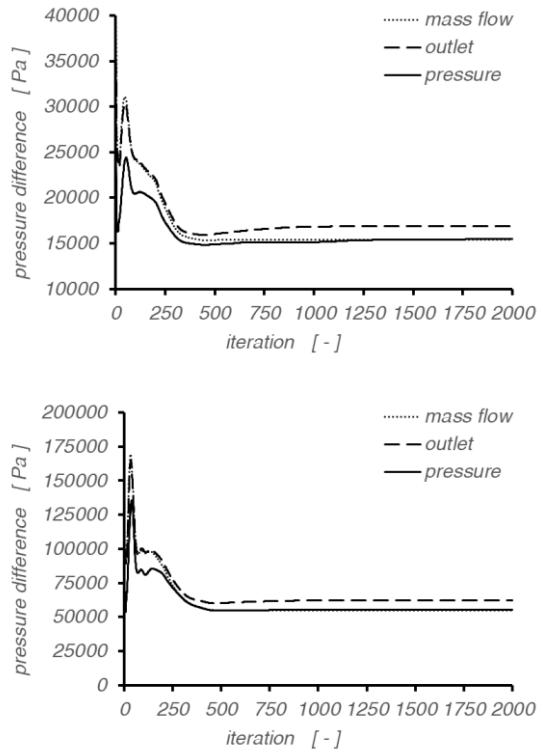

Figure 5. History of the pressure difference at the monitoring points, calculated for different types of outflow boundary condition: Q=15 m^3/s (above) and Q=35 m^3/s (below)

The computational results obtained by LES reveal that the flow exhibits small unsteady effects. In Figure 6, history of the pressure difference is shown. In the period from 0 *s* to 2 *s*, the flow is calculated using the 1st-order accurate upwind scheme for discretization of the convective term in the momentum-balance equation to promote stability and damping with the relatively coarse time step. From 2 *s* to 2.5 *s* of simulated time, discretization scheme for the convective term is switched to the 2nd-order accurate linear-upwind scheme, and after 2.5 *s* of simulated time the discretization scheme of inertial term is also switched to the 2nd-order accurate one, with the time step reduced to 0.001 *s*. Consequently, the simulation detects slight oscillations of the pressure difference between the monitoring points about 0.314 *bar* for the flow rate of 25 m^3/s. Fluctuations of the pressure difference amount to less than 0.5 %, which can be regarded as negligible. Also, a look at the pressure field, such as shown in Figure 7 for a typical instant of time, implies that the monitoring pressure locations are installed in the region of stable, non-fluctuating flow.

4. CONCLUSIONS

Water flow through the spiral casing of a hydraulic turbine is simulated using a computer program for CFD analysis. For the given range of water flow rates static pressure at the pre-defined monitoring points is calculated. The results of numerical simulation with the created computational model give a very good agreement with the measured pressure values. Thus, a relation between the pressure difference at the monitoring points and the incoming flow rate is established. This relation can be used for continuous estimation of the water flow rate in the turbine in operating conditions, by measuring static pressure at the given points.

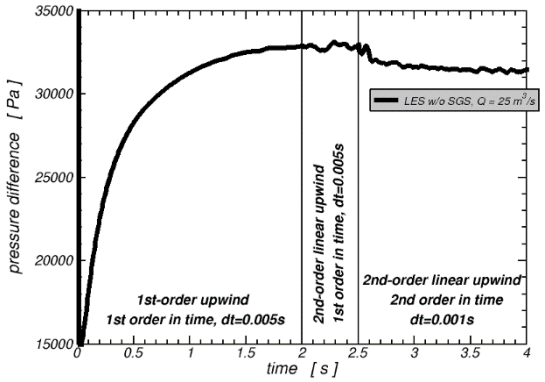

Figure 6. History of the pressure difference at the monitoring points, calculated with LES w/o SGS for Q=25 m^3/s

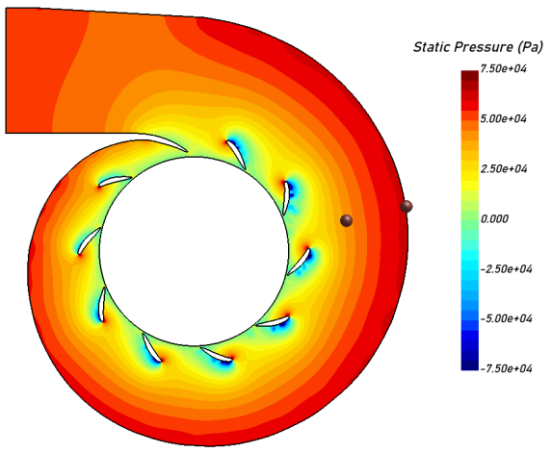

Figure 7. Instantaneous static-pressure field from LES w/o SGS, with the pressure monitoring locations indicated

Since the computational domain includes only inlet pipe, spiral casing, and the stay-vanes ring, for proper simulation appropriate boundary condition is needed at the outflow surface (downstream the stay

vanes). Imposed surface-averaged pressure at the outflow boundary gives the best agreement with the reference data. Testing different turbulent handling approaches did not give substantial differences. Based on the authors' experience, realizable k-ε can model can be adopted for steady-state runs or unsteady runs with relatively slow dynamics, and LES w/o SGS modelling with at least 2nd-order accurate discretization in space and time can be used for the simulations, where small-scale time variations of the flow properties are analysed.

ACKNOWLEDGEMENTS

Financial support is provided by Federal Ministry of Education and Science of FBiH, Bosnia and Herzegovina in year 2023, contract no. 05-35-2489-1/23 from 06.10.2023, which is gratefully acknowledged.

REFERENCES

[1] Winter, I.A., and Kennedy, A.M., 1933, „Improved type of flow meter for hydraulic turbines", *ASCE Proceedings*, Vol. 59, No. 4, Part 1, pp. 563-584.

[2] International Electrotechnical Commission, 1991, "Field acceptance tests to determine the hydraulic performance of hydraulic turbines, storage pumps and pump-turbines", *International Standard* IEC 60041:1991 (E), 3rd edition, Geneva, Switzerland.

[3] Baidar, B., Nicolle, J., Trivedi, C., and Cervantes, M.J., 2016, "Winter-Kennedy method in hydraulic discharge measurement: Problems and Challenges", *11th International conference on hydraulic efficiency measurement*, IGHEM 2016.

[4] Baidar, B., Nicolle, J., Trivedi, C., and Cervantes, M.J., 2018, "Numerical Study of the Winter-Kennedy Method – A Sensitivity Analysis", *Journal of Fluids Engineering*, Vol. 140, No. 5, 051103.

[5] Baidar, B., Nicolle, J., Gandhi, B.K., and Cervantes, M.J., 2020, "Numerical Study of the Winter–Kennedy Flow Measurement Method in Transient Flows", *Energies*, Vol. 13, No. 6, 1310.

[6] Rau, T., and Eissner, M., 2014, „Experience with Winter-Kennedy coefficients on hydraulic identical units", *The 10th International conference on hydraulic efficiency measurements*, IGHEM 2014.

[7] Baidar, B., Nicolle, J., Gandhi, B. K., and Cervantes, M. J., 2020, „Effects of runner change on the Winter-Kennedy flow measurement method – A numerical study", *Renewable Energy*, Vol. 153, pp. 975-984.

[8] Swain, T.K., Garimella, R., and Rahman, M. F., 2025, "Winter Kennedy Method — An Online Tool for Efficiency Monitoring of Hydro Power Plants", In: Pandey, M., Umamahesh, N., Das, J., and Pu, J.H. (eds) *Hydrology and Hydrologic Modelling*, *HYDRO 2023*, Lecture Notes in Civil Engineering, Vol. 410, Springer, Singapore.

[9] Siemens, *Simcenter STAR-CCM+ User Guide*.

[10] Shih, T.-H., Liou, W.W., Shabbir, A., Yang, Z., and Zhu, J., 1994, "A New k- Eddy Viscosity Model for High Reynolds Number Turbulent Flows – Model Development and Validation", *NASA Technical Memorandum*, 106721, ICOMP-94-21, CMOTT-94-6.

[11] Menter, F.R., 1994, "Two-equation eddy-viscosity turbulence modeling for engineering applications", *AIAA Journal*, Vol. 32, No. 8, pp. 1598-1605.

[12] Manceau, R., and Hanjalić, K., 2002, "Elliptic blending model: A new near-wall Reynolds-stress turbulence closure", *Physics of Fluids*, Vol. 14, No. 2, pp. 744-754.

[13] Patankar, S., 1980, *Numerical Heat Transfer and Fluid Flow*, CRC Press.

[14] Ferziger, J.H., Perić, M., and Street, R.L., 2020, *Computational Methods for Fluid Dynamics*, 4th ed., Springer.

[15] Hottinger, Brueel and Kjaer GmbH, *CATMAN, Operating Manual*.